Volume 24, No 4 | International Journal of Radiation Research, October 2026

Patient-derived three-dimensional bioprinted models of low-grade glioma: A pilot feasibility study

B. Hu[1#], S. Yang[1#], Z. Zhang[2], Y. Liu[1], D. Jiang[2*], J. Yang[3*]

[1]*Department of Neurosurgery, the First Affiliated Hospital of Sun Yat-sen University, Guangzhou, Guangdong, China*
[2]*CD BioEng & Therapy Co. Ltd, Ningbo, Zhejiang, China*
[3]*Department of oncology, Sichuan Provincial People's Hospital, University of Electronic Science and Technology of China, Chengdu, China*

► ***Original article***

***Corresponding author:**
Jia Yang, M.D.,
Dacheng Jiang, M.D.
E-mail:
yangj583@alumni.sysu.edu.cn
jiangdacheng@nb-changdu.com

Received: June 2026
Final revised: July 2026
Accepted: July 2026

Int. J. Radiat. Res., October 2026; 24(4): 969-979

DOI: 10.61186/ijrr.24.4.6

Keywords: *Low-grade glioma, patient-derived organoid, 3D bioprinting, in-vitro model, tumor microenvironment.*

[#]These authors contributed equally to this work.

ABSTRACT

Background: Patient-derived three-dimensional (3D) models may improve preclinical research of low-grade gliomas (LGGs), but the feasibility of bioprinting adult LGG tissue is poorly defined. ***Materials and Methods:*** Fresh surgical specimens from three patients with CNS WHO grade 2, IDH1-mutant gliomas were mechanically and enzymatically dissociated and incorporated into 7.5% or 8% gelatin methacryloyl bioinks. Constructs personalized to the patient were generated by extrusion bioprinting and cultured under physiological hypoxia for 35 days. Serial bright-field microscopy was used to assess morphological development and structural integrity. Intracellular ATP was measured longitudinally as an indirect marker of viable, metabolically active cells. ***Results:*** All three samples were successfully bioprinted into constructs. In the model from patient 1, tumor cells aggregated gradually during early culture and formed compact spheroid- or organoid-like structures by day 6–9. The printed architecture remained visible up to day 35 without apparent macroscopic collapse or total disintegration. In both GelMA formulations, the ATP-associated chemiluminescence in the Patient 1-derived model was not diminished as compared to the baseline at day 3 and remained high throughout the observation period, indicating persistent metabolic viability. The available data did not allow for a definitive comparison between the two concentrations of GelMA, nor for an evaluation of reproducibility across all patients. ***Conclusion:*** Patient-derived LGG cells can be encapsulated in 3D bioprinted GelMA constructs and cultured in-vitro for up to 35 days. These findings support technical feasibility and warrant validation in larger cohorts with molecular-fidelity and drug-response analyses.

INTRODUCTION

Low-grade gliomas (LGG) are a heterogeneous category of primary central nervous system tumors with slow growth, widespread infiltration, specific molecular changes and a continuous risk of recurrence and malignant progression. Low-grade gliomas have an indolent history but are difficult to treat. This is because the biological behavior is quite diverse from patient to patient and cannot be anticipated by histological classification alone. Molecular features like isocitrate dehydrogenase 1/2 mutations, ATRX mutations, TP53 mutations and 1p/19q codeletion have improved tumor classification and prognostic assessment but there is still a paucity of clinically relevant models that accurately reproduce the biology of individual tumors.

Traditionally preclinical glioma research has been based on immortalized cell lines, genetically modified mice models and patient-derived xenografts. Standard 2D cell cultures are experimentally tractable and amenable to high-throughput assays, but long-term *in-vitro* propagation may lead to genetic drift, phenotypic selection, and loss of the cellular heterogeneity and tissue architecture present in the original tumor. Genetically engineered mouse models can replicate specific oncogenic alterations such as IDH-associated tumorigenesis but suffer from long model development times, high maintenance costs and lack of heterogeneity in genetic make-up and tumor microenvironment that is seen in human gliomas. Such restrictions may be among the reasons for the poor translation of promising preclinical discoveries into clinically effective medicines [1-3].

One interesting technique to overcome some of these restrictions is development of patient derived three-dimensional culture models. Organoid systems offer controlled experimental modification and retain important histologic, genetic, metabolic and cellular properties of the original tumor. Abdullah *et al.* established patient-derived organoid models of lower grade gliomas from whole tumor tissue in physiologic hypoxia without adding exogenous extracellular matrix. This paradigm kept important molecular changes and intratumoral heterogeneity intact, especially in adult IDH-mutant gliomas [4]. Adult IDH-mutated tumors may lose their specific genetic traits

[Downloaded from mail.ijrr.com on 2026-11-11]

[DOI: 10.61186/ijrr.24.4.6]

under these conditions, but alternative techniques like as conditional reprogramming culture have allowed some pediatric and compact low-grade gliomas to proliferate fast and persist over time [5]. Recently, organoid platforms that recreate the glioma microenvironment have been proven to be promising for maintaining endogenous stromal and immunological components and evaluating personalized treatment [3, 6].

However, existing organoid models have several key limitations including variable success in establishing models, variable composition of the extracellular matrix, long preparation times, limited control of spatial organization, and difficulty in maintaining non-neoplastic components of the tumor microenvironment. These concerns are particularly important for LGGs which often develop slower than high grade gliomas and hence may require longer culture durations before adequate material is available to perform functional tests. An evaluation model for individualized treatments must not only preserve the biological properties of the source tumour, but also be produced fast enough and reproducibly enough to be relevant for clinical decision-making.

Three-dimensional bioprinting is an alternative that enables controlled placement of patient-derived tumor cells in scaffolds based on biomaterials. This technique makes it possible to produce reproducible constructions with controlled 3D architecture and microenvironmental features by tuning the composition, concentration, mechanical properties and spatial distribution of bioinks. Hydrogel materials such as gelatin methacryloyl and hyaluronic acid-based matrices have been employed to facilitate glioma-cell aggregation, clonal sphere formation, and drug-response evaluation [7, 8]. Bioprinted glioblastoma models and glioblastoma-on-a-chip systems have also been able to recapitulate oxygen gradients, tumor-stroma interactions, and patient-specific responses to chemoradiotherapy [9, 10]. In addition, promising feasibility and potential clinical concordance of patient-derived 3D bioprinted models were shown for a number of extracranial malignancies including, among others, hepatocellular, gastric, colorectal, pancreatic and gastrointestinal stromal tumors [11-15].

However, there is limited evidence supporting the fabrication and sustained culture of patient-derived 3D-bioprinted models specifically in LGGs. Most current bioprinting studies have focused on glioblastoma or other rapidly proliferating cancers and it is unknown whether the same strategies can support long term viability and structural organization of low-grade glioma cells. The feasibility of this approach should be proved before examining its applicability for drug screening, tumor evolution or tailored therapy prediction.

In this pilot investigation, we developed patient-specific 3D-bioprinted models from fresh surgical specimens of three patients with histologically and molecularly defined WHO grade 2 gliomas. The technical feasibility of model production was investigated, short- and long-term morphological development was described and longitudinal cellular viability was assessed by ATP-based tests. We anticipated that patient-derived LGG cells may be incorporated into hydrogel-based bioprinted constructions with maintenance of 3D structural integrity and sustained vitality throughout long-term *in-vitro* culture.

To our knowledge, this study represents one of the first pilot investigations specifically evaluating the construction and prolonged maintenance of patient-derived three-dimensional bioprinted models from adult CNS WHO grade 2, IDH1-mutant gliomas. Unlike previous studies predominantly focused on glioblastoma or extracranial malignancies, the present work evaluates whether slowly proliferating low-grade glioma cells can withstand tissue dissociation, GelMA incorporation, extrusion bioprinting, photocrosslinking, and culture for up to 35 days. The study further provides a preliminary comparison of 7.5% and 8% GelMA formulations and longitudinal ATP-based viability assessment.

MATERIALS AND METHODS

Study design

This study was designed as a pilot laboratory feasibility investigation to evaluate the construction and longitudinal maintenance of patient-derived three-dimensional bioprinted models of low-grade glioma. Fresh tumor tissues obtained during surgical resection were used to generate patient-specific bioprinted constructs. The feasibility of model establishment was assessed using serial bright-field microscopy and longitudinal measurements of intracellular adenosine triphosphate content.

The study included tumor specimens from three patients with histologically confirmed World Health Organization grade 2 gliomas: one astrocytoma and two oligodendrogliomas, including one recurrent oligodendroglioma. All three tumors harbored an IDH1 mutation.

Ethical approval and informed consent

The study protocol was reviewed and approved by the Institutional Review Board or Ethics Committee of First Affiliated Hospital of Sun Yat-Sen University under. Written informed consent was obtained from all participants before the collection and experimental use of surgical tumor tissue. Consent was also obtained for the use and publication of anonymized clinical, radiological,

[Downloaded from mail.ijrr.com on 2026-11-11]

[DOI: 10.61186/ijrr.24.4.6]

histopathological, and molecular data. All study procedures were conducted in accordance with the Declaration of Helsinki and applicable institutional and national ethical requirements.

Patient selection

Patients undergoing surgical resection for a suspected low-grade glioma were considered eligible for inclusion.

The inclusion criteria were age of at least 18 years, surgical resection of a radiologically suspected low-grade glioma, availability of sufficient fresh tumor tissue for experimental processing, histopathological confirmation of a WHO grade 2 glioma; and, and availability of relevant clinical, radiological, and molecular pathological information.

Patients with inadequate tissue volume or quality for model construction, extensive tissue necrosis, contamination or substantial delay between resection and laboratory processing, final diagnosis other than low-grade glioma and absence of informed consent were excluded.

Patients were enrolled using a convenience sampling approach.

Clinical and radiological assessment

Demographic and clinical information was obtained from the patients' medical records. Recorded variables included age, sex, tumor location, previous glioma diagnosis or treatment, histological diagnosis, WHO grade, and molecular pathological features.

All patients underwent preoperative magnetic resonance imaging. The MRI protocol included at least T1-weighted, T2-weighted, and post-contrast T1 -weighted imaging. Additional sequences, including fluid-attenuated inversion recovery, diffusion-weighted imaging, susceptibility-weighted imaging, or perfusion imaging, were obtained according to the institutional clinical protocol.

The radiological features evaluated included tumor location, maximum dimensions, signal intensity on T1- and T2-weighted images, contrast-enhancement pattern, and evidence of postoperative or recurrent disease. Representative preoperative MRI images were selected for presentation.

Patient 1 had a non-enhancing lesion in the left parietal lobe measuring approximately 4.2 × 3.6 × 4.2 cm. Patient 2 demonstrated postoperative changes and a non-enhancing abnormal signal area in the left frontal lobe measuring approximately 4.8 × 1.7 cm, suggesting recurrent glioma. Patient 3 had a right frontal lesion measuring approximately 2.5 × 2.1 × 1.9 cm with mild focal enhancement.

MRI examinations were reviewed by 2 neuroradiologist(s) with 10 years of experience. The reviewers were blinded to the experimental findings.

Histopathological and molecular classification

At the department, neuropathologists analyzed the tumor tissues that were removed. The histopathological and molecular diagnoses were made according to the 2021 WHO Classification of Tumors of the Central Nervous System [16]. Formalin-fixed paraffin-embedded tissue slices were stained with hematoxylin-eosin and analyzed by immunohistochemistry. The indicators assessed included glial fibrillary acidic protein, OLIG2, mutant IDH1, p53, Ki-67, ATRX, SOX10 and CDKN2A where clinically appropriate. The method of 1p/19q codeletion determination was [fluorescence in situ hybridization / polymerase chain reaction / next generation sequencing / other]. [Immunohistochemistry / sequencing technique] was used to assess the status of IDH mutation. The techniques utilized to analyze ATRX, CDKN2A and other molecular changes should also be mentioned.

Patient 1 had a diagnosis of IDH1-mutant astrocytoma, CNS WHO grade 2, with loss of ATRX, p53 expression in approximately 50% of tumor cells, and a Ki-67 index of 2%. Patient 2 was diagnosed with recurrent IDH1-mutant oligodendroglioma, CNS WHO grade 2, with preserved ATRX expression, wild-type p53 expression pattern, Ki-67 index of 10% and negative CDKN2A evaluation. Patient 3: IDH1-mutant oligodendroglioma, CNS WHO grade 2, retained ATRX expression, wild-type p53 expression pattern, 1% Ki-67 index, SOX10 positivity, and 1p/19q codeletion.

Collection and transport of tumor tissue for surgical operation

A viable portion of the tumor was selected by the operating neurosurgeon or neuropathologist immediately after surgical resection. Areas of significant bleeding, coagulation damage, or macroscopic necrosis are avoided. Each specimen was placed in a sterile container and was transported to the laboratory within approximately 10 min after resection. Samples of the three patients were processed separately to prevent cross contamination. The approximate mass or dimensions of tissue used to build the model should be recorded for each patient.

Tumor-tissue dissociation and cell preparation

Fresh surgical tumor specimens were dissociated by a combination of mechanical and enzymatic methods. In brief, specimens were washed twice with ice-cold calcium- and magnesium-free phosphate-buffered saline and mechanically minced into ~1-mm 3 fragments with sterile scalpels and surgical forceps. The minced tissue was incubated in Dulbecco's modified Eagle medium/F12 with 1 mg/mL collagenase type IV (Gibco, Thermo Fisher Scientific; cat. no. 17104019) and 100 μg/mL DNase I (Sigma-

[Downloaded from mail.ijrr.com on 2026-11-11]

[DOI: 10.61186/ijrr.24.4.6]

Aldrich; cat. no. D5025) at 37°C for 30 min with gentle continuous agitation. The suspension was gently triturated every 10 min during incubation with a wide-bore pipette for tissue dissociation, minimizing mechanical damage to the cells. Enzymatic digestion was stopped by addition of an equal volume of ice-cold complete DMEM/F12 with 10% fetal bovine serum. The resultant cell suspension was passed through a 70-µm sterile cell strainer to eliminate undigested tissue fragments and cellular debris, and then centrifuged at 300 × g for 5 min at room temperature. The supernatant was removed and the cell pellet was re-suspended in serum-free DMEM/F12 culture medium.

When substantial erythrocyte contamination was observed, red blood cells were removed by incubating the cell pellet with 1× ammonium-chloride–potassium lysing buffer (Gibco, Thermo Fisher Scientific; catalogue no. A1049201) for 2 minutes at room temperature. Lysis was terminated by adding excess phosphate-buffered saline, followed by centrifugation at 300 × g for 5 minutes. Cell number and initial viability were determined using trypan blue exclusion with an automated cell counter. Only cell suspensions with an initial viability of at least 80% were used for bioprinting. The final cell concentration used for bioink preparation was adjusted to 1×10^6 viable cells/mL.

Preparation of the hydrogel-based bioink

Patient-derived tumor cells were dissociated and combined with a biocompatible hydrogel-based bioink prior to printing. Two formulations of gelatin methacryloyl were tested: 7.5% and 8% (w/v) final concentration. Sterile lyophilized GelMA with intermediate degree of methacryloyl substitution was purchased from Engineering for Life Co., Ltd. (EFL-GM-60; Suzhou, China). GelMA was dissolved in calcium and magnesium free Dulbecco's PBS at 50°C for ~30 min under gentle mixing until a homogenous solution was obtained. All preparations were carried out under sterile conditions and in the dark.

A photoinitiator, lithium phenyl-2,4,6-trimethylbenzoylphosphinate (LAP; Engineering For Life Co., Ltd., Suzhou, China) was added to a final concentration of 0.06% (w/v). The GelMA-LAP solution was filtered with a sterile 0.22 µm syringe filter prior to cell incorporation. Published glioma hydrogel and bioprinting studies have used GelMA-based formulations selected to balance printability, structural stability, and cytocompatibility [8, 10]. The prepared patient-derived tumor-cell suspension was then mixed with the GelMA precursor solution to a final density of 1× 10 6 viable cells/mL. The mixture was added dropwise using a wide-bore pipette tip to ensure homogenous distribution of cells, to reduce air bubble formation, cell sedimentation and mechanical cell damage. Cells were suspended in the bioink and cooled down to ~20 °C for 2–3 min to make the viscosity suitable for extrusion. The temperature of the mixture was maintained at ~37 ° C.

The 7.5% and 8% GelMA formulations were selected because GelMA concentrations in this range are sufficiently viscous and stable after cross-linking for extrusion printing while allowing for nutrient diffusion, cell spreading, aggregate formation and proliferation. Previous studies have evaluated GelMA concentrations within this range for glioma modeling and reported favorable printing fidelity and cellular compatibility [8,10]. In this pilot study, we compared the two concentrations close in concentration to preliminarily assess whether a modest change in hydrogel concentration affected the structural stability or viability of patient-derived LGG constructs.

Three-dimensional bioprinting

Patient-specific low-grade glioma constructs were fabricated in a sterile environment of a Class II biological safety cabinet using an EFL-BP6601 extrusion-based three-dimensional bioprinter (Engineering for Life Co., Ltd., Suzhou, China). Each patient sample and GelMA concentration was printed using a dedicated sterile printing cartridge and nozzle to avoid cross-contamination. The cell-laden bioink was then transferred into a sterile 3-mL printing cartridge, equipped with a blunt 22-gauge conical nozzle, with an internal diameter of about 410 µm. The loaded cartridge was kept at 20 °C for about 3 min before printing to stabilize the viscosity of the GelMA bioink. No bubbles were seen and prior to model fabrication the extrusion was continuous without restriction.The constructs were printed in a lattice pattern perpendicular to the filament with the initial parameters:

- Nozzle internal diameter: ~ 410 µm Extrusion pressure: 40 kPa.
- Print Speed: 5mm/sec; Layer height: 0.30 mm; Number of printed layers: 4;
- build dimensions: 10 by 10 by 1.2 mm^3;
- Bioink cartridge temperature: 20°C; and Printing-bed temperature: 15°C.

The extrusion pressure was adjusted within a narrow range of around 35–45 kPa if needed for a continuous filament without interruption or excessive spreading. Printing speed and other geometric parameters were the same in the 7.5% and 8% GelMA groups. Previously published glioma-bioprinting protocols have used comparable extrusion speeds, nozzle diameters, bioink temperatures, and lattice dimensions [10].

The constructs were photocrosslinked immediately after printing with a 405 nm visible-light -emitting diode with an intensity of approximately 25 mW/cm2 for 20 sec. The light source was positioned at ~3 cm above the printed construct for even crosslinking. Visible-light activation of LAP at 405 nm

[Downloaded from mail.ijrr.com on 2026-11-11]

[DOI: 10.61186/ijrr.24.4.6]

is often used for rapid GelMA solidification, however, excess photoinitiator concentration or prolonged irradiation should be avoided as both can have detrimental effects on cell viability.

After the crosslinking step, the constructs were gently rinsed once with pre-warmed culture medium to remove any unreacted material and immediately placed into complete culture medium. Each individual patient was a biological replicate. For each patient, three constructs printed independently were generated for the 7.5% GelMA condition, and three for the 8% GelMA condition, for a total of six technical replicate constructs per patient, and 18 constructs overall. ATP measurements were performed in triplicate constructs per patient and condition at each available assessment point or according to the available experimental design. Before analysis, constructs were excluded based on incomplete extrusion, marked discontinuity of printed filaments, collapse or major deformation immediately after printing, visible contamination, extensive cell leakage, insufficient cellular content or inadvertent deviation from the predefined printing or crosslinking parameters.

In-vitro culture of bioprinted constructs

Following photocrosslinking, the printed constructs were gently washed once with prewarmed culture medium and individually transferred into 24-well ultra-low-attachment culture plates (Corning Costar, Corning Incorporated, Corning, NY, USA). Each well contained 1 mL of serum-free glioma organoid culture medium.

The basal culture medium consisted of a 1:1 mixture of Dulbecco's modified Eagle medium/F12 and Neurobasal medium supplemented with 1× GlutaMAX, 1× minimum essential medium non-essential amino acids, 1× N-2 supplement, 1× B-27 supplement without vitamin A, 100 U/mL penicillin, 100 µg/mL streptomycin, 55 µM 2-mercaptoethanol, and 2.5 µg/mL recombinant human insulin. No serum or exogenous epidermal growth factor or fibroblast growth factor was added. This formulation was selected because a comparable serum-free medium has been used to maintain patient-derived lower-grade glioma organoids while limiting the selective pressure associated with serum-containing or mitogen-rich media [4].

The constructs were maintained under static culture conditions at 37°C in a humidified incubator containing 5% CO_2 and 5% O_2. Approximately 75% of the culture medium was replaced every 48 hours with freshly prepared, prewarmed medium. During medium replacement, the medium was aspirated carefully from the edge of the well to avoid disrupting or aspirating the bioprinted construct. Physiological hypoxia was selected because previous patient-derived LGG organoid studies demonstrated improved long-term structural preservation under 5% rather than atmospheric oxygen conditions [4].

The total observation period was 35 days. Constructs were inspected during every medium change for contamination, detachment, collapse, fragmentation, or other evidence of structural deterioration.

Morphological evaluation

The morphology and structural integrity of the bioprinted constructs were evaluated longitudinally using an Olympus CKX53 inverted bright-field microscope equipped with an Olympus DP22 digital camera (Olympus Corporation, Tokyo, Japan). Images were acquired using 4× and 10× objectives under standardized illumination, exposure, magnification, camera-gain, and white-balance settings. The same acquisition parameters were maintained across patients, GelMA concentrations, and observation time points.

Early morphological development was evaluated on culture days 1, 3, 6, and 9. For each time point, low-magnification images were acquired to document the overall printed architecture, whereas corresponding high-magnification images were obtained to assess tumor-cell distribution, aggregation, and spheroid- or organoid-like formation. Scale bars of 200 µm and 100 µm were used for low- and high-magnification images, respectively.

Long-term structural integrity was evaluated on culture days 15, 23, 31, and 35 using the same microscopy and image-acquisition settings. The following morphological characteristics were assessed:

1. Overall integrity and continuity of the printed construct;
2. Distribution of tumor cells within the hydrogel;
3. Formation, number, and size of cellular aggregates;
4. Development of spheroid- or organoid-like structures;
5. Presence of cellular outgrowth or migration within the hydrogel;
6. Construct contraction, deformation, fragmentation, or disintegration; and
7. Presence of extensive cellular debris or microbial contamination.

Morphological assessment was independently performed by two investigators who were blinded to patient identity and GelMA concentration. Disagreements were resolved by joint review and consensus. Quantitative image analysis was performed using ImageJ software, version 1.54f (National Institutes of Health, Bethesda, MD, USA). For each construct and time point, three non-overlapping representative fields were analyzed at the same magnification. Images were calibrated using the microscope scale bar, converted to 8-bit format, and subjected to a standardized background-subtraction and thresholding procedure. The following parameters were recorded:

[Downloaded from mail.ijrr.com on 2026-11-11]

[DOI: 10.61186/ijrr.24.4.6]

- Number of cellular aggregates per field;
- Mean aggregate area in μm^2;
- Equivalent aggregate diameter in μm;
- Percentage of the analyzed field occupied by cellular aggregates; and
- Relative construct area compared with day 1.

Aggregate boundaries were manually corrected when automated thresholding failed to separate adjacent structures. ImageJ is an established open-source platform for quantitative biological image analysis.

ATP-based cell-viability assay

Cell viability within the bioprinted constructs was evaluated by measuring intracellular ATP using the CellTiter-Glo 3D Cell Viability Assay (Promega Corporation, catalogue no. G9681, Madison, WI, USA). ATP-dependent chemiluminescence was used as an indirect measure of the number and metabolic activity of viable cells. The CellTiter-Glo 3D formulation was selected because it has enhanced lytic capacity and is specifically designed for ATP quantification in three-dimensional cell cultures.

ATP measurements were performed on culture days 3, 6, 9, 12, 15, 23, 27, 31, and 35. Because the assay required complete lysis of the construct, separate constructs were allocated to each GelMA concentration and assessment time point, and an assayed construct was not returned to culture or reused at a subsequent time point.

At each assessment time point, the culture plate and CellTiter-Glo 3D reagent were equilibrated to room temperature for 30 minutes. An equal volume of CellTiter-Glo 3D reagent was added directly to the culture medium in each well. The plate was mixed vigorously on an orbital plate shaker for 5 minutes to promote disruption of the hydrogel and cellular lysis and was subsequently incubated at room temperature for 25 minutes to allow stabilization of the luminescent signal.

Following incubation, 100 μL of the resulting lysate was transferred into each of three wells of an opaque white 96-well assay plate. Chemiluminescence was measured using a GloMax Discover multimode microplate reader (Promega Corporation, Madison, WI, USA) with an integration time of 1 second per well. The three readings obtained from each construct were averaged to produce one value for that construct. The assay procedure, including equal-volume reagent addition, extended mixing, and incubation before measurement, followed the manufacturer's recommendations for three-dimensional cultures.

For each GelMA concentration and time point, three independently printed constructs were analyzed as experimental replicates. Three aliquots from each construct lysate were measured as technical plate-reading replicates. Technical readings from the same construct were averaged and were not treated as independent experimental observations.

Cell-free constructs prepared using the corresponding 7.5% or 8% GelMA formulation were cultured and assayed under identical conditions. Mean luminescence from the matched cell-free hydrogel controls was subtracted from the corresponding cell-containing construct values to correct for background signal.

Background-corrected ATP values were initially reported as relative luminescence units per construct. For longitudinal presentation, the mean ATP value obtained on day 3 for each GelMA concentration was defined as 100%, and subsequent values were calculated as follows:

Relative ATP activity (%) = (background-corrected ATP at the specified time point ÷ mean background-corrected ATP on day 3 for the corresponding GelMA concentration) × 100.

The source manuscript presents longitudinal ATP findings only for the bioprinted model derived from patient P1. Accordingly, ATP results should be described as originating from P1 unless equivalent measurements were obtained and documented for patients P2 and P3.

Study outcomes

The primary endpoint was technical feasibility of a patient derived 3D-bioprinted low grade glioma construct from freshly resected tumor tissue. Successful model construction was defined as:

1. Printing and cross-linking are completed without serious structural failure;
2. retention of tumor cells in the hydrogel construct;
3. preservation of a discernible three-dimensional architecture during culture; and
4. demonstration of viable cellular activity following model establishment.

Secondary outcomes included

1. Formation of tumor-cell aggregates or spheroid / organoid-like structures;
2. Maintenance of structural integrity up to day 35;
3. Variation of ATP-associated chemiluminescence with time;
4. Viability variations between the 7.5% and 8% GelMA formulations; and
5. Incidence of model failure, disintegration or contamination.

Drug-response experiments and direct molecular comparisons between the parental tumors and the bioprinted constructs were not reported and thus were not considered outcomes of this pilot study.

Statistical analysis

Given the exploratory nature of the study and the inclusion of only three patient-derived samples, the analysis was primarily descriptive.

[Downloaded from mail.ijrr.com on 2026-11-11]

[DOI: 10.61186/ijrr.24.4.6]

Patient characteristics were presented individually. Continuous variables were summarized using mean and standard deviation where appropriate. Categorical variables were reported as counts and percentages.

ATP-associated chemiluminescence values were reported as [mean ± standard deviation/median and interquartile range] across replicate constructs at each time point. Values may also be expressed relative to the day 3 baseline using the following calculation:

Relative ATP activity (%) = (ATP value at the specified time point / ATP value on day 3) × 100.

Changes over time and differences between the 7.5% and 8% GelMA conditions were analyzed using [statistical method], provided that a sufficient number of independent biological replicates were available. Technical replicates derived from the same patient specimen were not treated as independent patient-level observations.

Because of the small number of patients, inferential results were considered exploratory, and no conclusions regarding clinical efficacy or generalizability were drawn. Statistical analyses were performed using R package. A two-sided P value of less than 0.05 was considered statistically significant only for prespecified exploratory comparisons.

RESULTS

Patient characteristics and molecular pathology

The study was a pilot trial and involved 3 adult patients with histologically confirmed CNS WHO grade 2 low grade gliomas (table 1). The group consisted of 2 men and 1 female aged 36–47 years. Astrocytoma was diagnosed in 1 patient and oligodendroglioma (recurrent tumor in 1 patient) in 2 patients. All the malignancies were found in the cerebral hemispheres and harbored an IDH1 mutation.

Patient 1 was a 47-year-old male with an astrocytoma localized to the left parietal lobe. The tumor was diagnosed as IDH1-mutant astrocytoma, CNS WHO grade 2 and was positive for GFAP, OLIG2 and mutant IDH1. Immunohistochemical examination showed p53 expression in ~50% of tumor cells, a Ki-67 proliferation index of 2% and decrease of ATRX expression.

Patient 2 was a 44-year-old male with a recurring oligodendroglioma in the left frontal lobe. The tumor was diagnosed as CNS WHO grade 2, IDH1-mutant. It was positive for GFAP, OLIG2 and mutant IDH1, with a wild-type p53 staining pattern, preserved ATRX expression, a Ki-67 proliferation score of 10% and negative CDKN2A evaluation.

Patient 3 was a 36-year-old female with an oligodendroglioma arising in the right frontal lobe. The tumor was positive for GFAP, OLIG2, mutant IDH1 and SOX10 and was CNS WHO grade 2, IDH1-mutant. It showed a wild-type p53 staining pattern, maintained ATRX expression, a Ki-67 proliferation index of 1%, and 1p/19q codeletion.

Preoperative MRI findings

Preoperative MRI demonstrated radiological features compatible with low-grade glioma in all three patients.

In Patient 1, MRI revealed a patchy abnormal signal lesion in the left parietal lobe measuring approximately 4.2 × 3.6 × 4.2 cm. The lesion was hypointense on T1-weighted imaging and hyperintense on T2-weighted imaging, without evident contrast enhancement. The imaging appearance was suggestive of adult diffuse astrocytoma.

In Patient 2, postoperative changes were observed in the left frontal lobe, together with an abnormal signal area measuring approximately 4.8 × 1.7 cm. The lesion was hypointense on T1-weighted imaging, hyperintense on T2-weighted imaging, and showed no contrast enhancement. These findings were considered suggestive of recurrent left frontal glioma.

In Patient 3, MRI showed a nodular lesion in the right frontal lobe measuring approximately 2.5 × 2.1 × 1.9 cm. The lesion was iso- to hypointense on T1-weighted imaging and iso- to hyperintense on T2-weighted imaging, with mild focal enhancement after contrast administration.

Representative MRI findings are presented in figure 1.

Feasibility of patient-derived 3D-bioprinted LGG model construction

Fresh surgical tumor tissue from each patient was processed by combined mechanical and enzymatic dissociation and subsequently incorporated into a hydrogel-based bioink. Patient-specific three-dimensional constructs were generated by extrusion bioprinting.

Bioprinted models were successfully established from all three patient specimens. Immediately after printing and crosslinking, the constructs demonstrated preserved overall geometry and satisfactory structural integrity. Tumor cells remained distributed within the hydrogel matrix, and no immediate disintegration of the printed architecture was observed.

The available manuscript does not report the number of failed constructs, contamination events, excluded specimens, or unsuccessful printing attempts. Therefore, a formal model-establishment success rate could not be calculated.

[Downloaded from mail.ijrr.com on 2026-11-11]

[DOI: 10.61186/ijrr.24.4.6]

Early morphological development of the bioprinted constructs

Serial bright-field microscopy revealed gradual cellular organization within the bioprinted hydrogel during the initial culture period. Representative images of the model derived from patient 1 were taken on culture days 1, 3, 6, and 9. On day 1, the tumor cells were found dispersed in the printed hydrogel. In the next culture, the cells gradually aggregated and formed more compact multicellular structures. On days 6 and 9, spheroid- or organoid-like aggregates were observed in the construct, showing that the environment of the hydrogel promoted three-dimensional cellular organization in the early period of culture. Low magnification images demonstrated preservation of overall printed architecture, whereas corresponding high magnification images revealed progressive cellular aggregation and spheroid-like formation. Figure 2 shows representative pictures of early-culture.

Long-term structural stability

The bioprinted LGG model maintained its three-dimensional architecture during prolonged *in-vitro* culture.

Representative bright-field images obtained from the Patient 1-derived model on days 15, 23, 31, and 35 demonstrated continued preservation of the printed structure. No evident macroscopic collapse or complete disintegration was observed during the 35-day observation period. Cellular aggregates remained visible within the hydrogel, and the construct retained overall structural continuity at the final assessment.

These observations indicate that the hydrogel-based bioprinted environment was capable of supporting the prolonged structural maintenance of patient-derived LGG cells. Representative long-term images are shown in figure 3.

Because no predefined quantitative structural-integrity score was reported, long-term stability was assessed qualitatively from serial microscopy.

Longitudinal ATP-based cell viability

Intracellular ATP levels as an indirect measure of viable and metabolically active cells within the bioprinted construct were measured longitudinally. The available ATP data were obtained from the model generated from patient 1 and had measurements on days 3, 6, 9, 12, 15, 23, 27, 31 and 35 of culture. The two concentrations of GelMA tested were 7.5% and 8%. The approximate cell-viability values for the 7.5% GelMA group at the nine time points were 145, 158, 191, 203, 199, 184, 214, 163 and 180, respectively. In the 8% GelMA group the corresponding values were approximately 101, 124, 130, 148, 149, 149, 162, 145 and 128. Thus, cell viability remained above the day 3 level throughout the study period for both formulations.

For the 7.5% GelMA constructs, the viability increased from approximately 145 on day 3 to 203 on day 12, corresponding to an increase of approximately 40.0%, and reached a peak of approximately 214 on day 27, representing an increase of approximately 47.6% relative to day 3. This viability decreased post but remained high at day 35 (~180) which was still about 24.1% higher than the initial day 3 level. For the 8% GelMA constructs, viability increased from ~101 at day 3 to 148–149 between days 12 and 23, corresponding to an increase of ~46–48%, and peaked at ~162 on day 27, representing an increase of ~60.4% relative to baseline. Day 35 showed viability decreased to approximately 128, which was still about 26.7% higher than day 3. 7.5% GelMA group showed statistically significant higher absolute ATP viability at all time points in culture compared to 8% GelMA group with absolute differences ranging from 17.8 to 60.8 units. The largest difference occurred around day 9, where the viability was around 191 in the 7.5% and 130 in the 8% group.

Table 1. Clinical and molecular features of three patients with low-grade gliomas.

Patient ID	Age (years)	Sex	Diagnosis	Surgical site	WHO grade	Molecular pathology
P1	47	M	Astrocytoma	Left parietal lobe	2	IDH1-mutant, CNS grade 2, GFAP (+), Oligo2 (+), IDH1 (+), p53 50%, Ki-67 2%, ATRX (loss).
P2	44	M	Oligoden-droglioma (recurrent)	Left frontal lobe	2	IDH1-mutant, CNS grade 2, GFAP (+), Oligo2 (+), IDH1 (+), p53 wild-type, Ki-67 10%, ATRX retained, CDKN2A (-).
P3	36	F	Oligoden-droglioma	Right frontal lobe	2	IDH1-mutant, CNS grade 2, GFAP (+), Oligo2 (+), IDH1 (+), SOX10 (+), p53 wild-type, Ki-67 1%, ATRX retained, 1p/19q codeletion.

Abbreviations: M, male; F, female; IDH, isocitrate dehydrogenase; CNS, central nervous system; GFAP, glial fibrillary acidic protein; Oligo2, oligodendrocyte transcription factor 2; ATRX, alpha-thalassemia/mental retardation syndrome X-linked; CDKN2A, cyclin-dependent kinase inhibitor 2A; SOX10, SRY-box transcription factor 10; 1p/19q codeletion, combined deletion of chromosome arms 1p and 19q.

[Downloaded from mail.ijrr.com on 2026-11-11]

[DOI: 10.61186/ijrr.24.4.6]

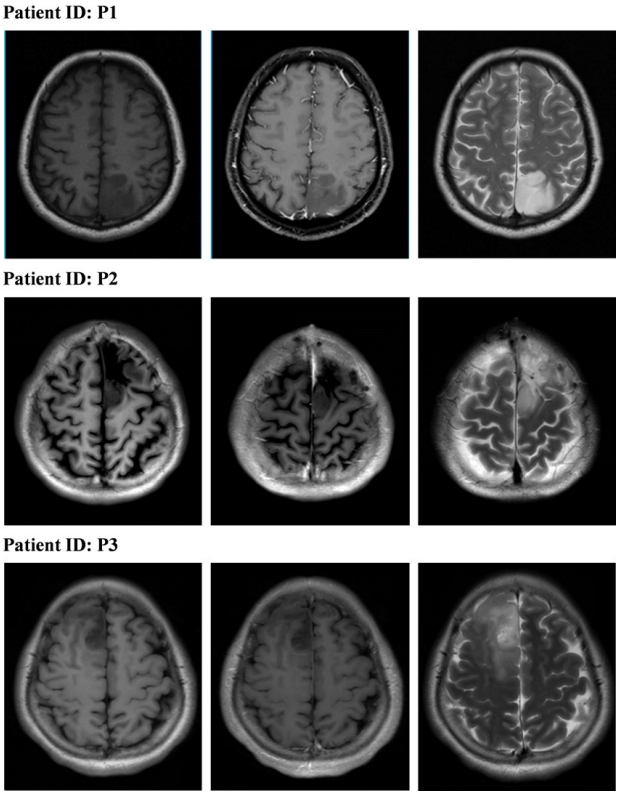


Figure 1. Preoperative MRI of three representative patients with low-grade gliomas. **(P1)** Imaging diagnosis: patchy-like abnormal signal lesion in the left parietal lobe, size approximately 4.2 cm × 3.6 cm × 4.2 cm, hypointense on T1WI, hyperintense on T2WI, no enhancement on contrast-enhanced scan; suggestive of adult diffuse astrocytoma. **(P2)** Imaging diagnosis: postoperative changes of left frontal lobe tumor, size approximately 4.8 cm × 1.7 cm, hypointense on T1WI, hyperintense on T2WI, no enhancement on contrast-enhanced scan; suggestive of possible recurrence of left frontal glioma. **(P3)** Imaging diagnosis: nodular abnormal signal lesion in the right frontal lobe, size approximately 2.5 cm × 2.1 cm × 1.9 cm, iso-/hypointense on T1WI, iso-/hyperintense on T2WI, mild focal enhancement on contrast-enhanced scan; suggestive of glioma.

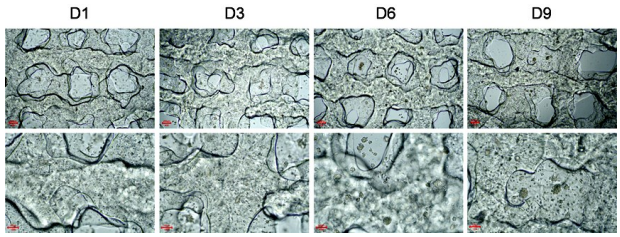


Figure 2. Bright-field images of a patient-derived 3D bioprinted LGG model. Bright-field images captured on culture days 1, 3, 6, and 9. For each time point, the upper row shows low-magnification views (scale bar = 200 μm), and the lower row shows corresponding high-magnification views (scale bar = 100 μm).

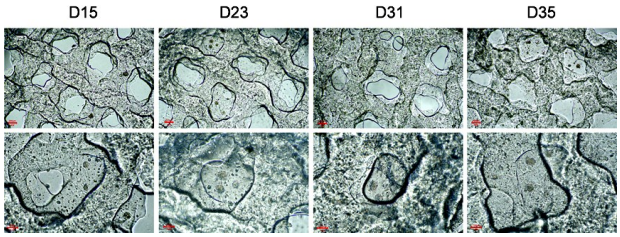


Figure 3. Long-term structural integrity of the 3D bioprinted LGG model. Bright-field images captured on culture days 15, 23, 31, and 35. For each time point, the upper row shows low-magnification views (scale bar = 200 μm), and the lower row shows corresponding high-magnification views (scale bar = 100 μm).

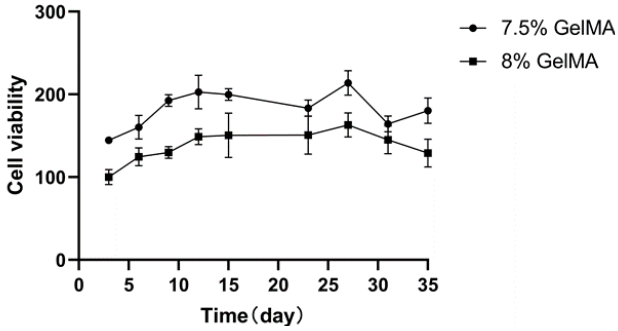


Figure 4. Cell viability of the 3D bioprinted LGG model derived from patient P1.

DISCUSSION

In this pilot feasibility study, patient-derived 3D-bioprinted models were established from fresh surgical specimens of three patients with CNS WHO grade 2, IDH1-mutant gliomas, one astrocytoma and two oligodendrogliomas (including one recurrent oligodendroglioma). Serial bright-field microscopy showed progressive cellular aggregation and spheroid- or organoid-like formation during early culture, and the constructs retained recognizable three-dimensional architecture for up to 35 days. Longitudinal ATP measurements in the Patient 1-derived model also indicated sustained metabolic viability throughout culture, with consistently higher values in the 7.5% GelMA formulation than in the 8% formulation.

These findings are indicative of the technical feasibility of tissue dissociation, GelMA incorporation, extrusion bioprinting, photocrosslinking and prolonged *in-vitro* culture of the patient-derived LGG cells. This is particularly important given the generally low proliferative activity of adult lower-grade gliomas, and their possible dependence on specific metabolic and microenvironmental conditions that may create difficulties in generating representative long-term models [2]. Our results are in line with previous studies of patient-derived LGG cultures. Abdullah *et al.* generated lower-grade glioma organoids by preserving intact tumor fragments in 5% oxygen without exogenous Matrigel, and the histological, genomic, cellular and metabolic features were maintained, particularly in adult IDH-mutant tumors [4]. This has permitted the propagation of selected low-grade gliomas, in particular pediatric compact

[Downloaded from mail.ijrr.com on 2026-11-11]
[DOI: 10.61186/ijrr.24.4.6]

tumors, but this approach does not recapitulate native three-dimensional architecture and may not adequately sustain adult IDH-mutant cells [5].

Organoids derived from fragments and bioprinted models offer complementary and distinct advantages. Organoids derived from fragments may more effectively retain the native cell-cell, cell-matrix, immune and stromal relationships. Bioprinting, however, is based on tissue dissociation that may disrupt the native spatial architecture and selectively remove fragile cell populations. However, bioprinting provides greater control over construct geometry, matrix composition, cell density, stiffness and spatial organization that may increase reproducibility and allow controlled investigation of specific microenvironmental variables.

Moreover, the formation of compact cellular aggregates within the GelMA hydrogel over time showed that the printed matrix promoted cell-cell interaction and 3D organization. Previous glioma-organoid experiments have showed that 3D culture inadequately recapitulates spatial gradients and cellular heterogeneity described in standard monolayer systems [1,17]. Glioma stem-cell survival, sphere formation and drug-response assessment have also been supported by scaffolds based on GelMA and hyaluronic acid [8]. However, rounded aggregates alone are not enough to prove the formation of biologically relevant organoids. Validation at the histological and molecular levels should include retention of lineage markers, proliferative states, characteristics of the extracellular matrix, and heterogeneity of the parental tumor. The ability to maintain structural integrity through day 35 represents a significant technological breakthrough as rapidly degrading constructs cannot support long term research of tumor evolution or treatment resistance. GelMA has variable mechanical and photocrosslinking capabilities to maintain print quality and permit transfer of nutrients and oxygen [7, 8]. However, physical stability does not ensure biological integrity, as tumor cells can be chosen, senescent, or phenotypically wander while the hydrogel stays intact.

For all GelMA formulations, ATP-related viability was maintained above the day 3 threshold throughout the investigation. The 7.5% formulation was more consistently metabolically active, suggesting that the lower polymer content may have been a more conducive environment for cell survival. However, ATP is an indicator of the viable cell number as well as the metabolic activity per cell and so cannot alone confirm proliferation. We should validate these observations with further assays such as Ki-67 or EdU labelling, DNA quantification, live/dead staining, apoptotic markers and quantitative longitudinal imaging. Additionally, ATP data were only provided for patient 1 and hence judgments on repeatability in astrocytoma and oligodendroglioma models are limited.

The difference between the two GelMA concentrations could be due to the differential in stiffness, pore size, nutrient diffusion, cell migration and hydrogel remodelling. Higher GelMA concentration can increase mechanical stability, but also limit cell migration and molecular diffusion. Lower concentrations can facilitate remodeling, but compromise print accuracy. Thus, the appropriate formulation should be identified by mechanical testing, shape fidelity assessment, degradation analysis, quantitative morphology, viability and molecular fidelity assessments. Composite bioinks using hyaluronic acid, laminin, collagen or brain-derived extracellular matrix can contribute to biological relevance [8, 9]. Another important question is the conservation of the IDH-mutant phenotype. Unlike other culture methods where IDH-mutant cells are selected against in long-term propagation [4, 5]. IDH1-mutant protein or mutant allele frequency, D-2-hydroxyglutarate production, ATRX status, TP53 changes, and 1p/19q codeletion were not evaluated following printing in this work. Hence, paired molecular comparison of parental tumors and corresponding constructs is important.

The cellular makeup of the bioprinted models is also unknown. Neoplastic cells in gliomas are accompanied by microglia, macrophages, lymphocytes, astrocytes, endothelial cells and other stromal components. Air–liquid interface and GlioME organoids have demonstrated partial conservation of endogenous immune and stromal populations, but these cells are difficult to maintain over time [3, 6]. Finally, bioprinting offers the possibility of tailored rebuilding of the microenvironment with specific cell populations as shown in more advanced glioma-bioprinting platforms [10]. However, it cannot yet be claimed that the current model is representative of the LGG microenvironment.

Patient-derived organoids and bioprinted tumor models have been shown to be promising tools for drug-response testing in glioma and several extracranial cancers [9-13,18]. However, drug exposure and comparison with patient outcome were not included in this study. Thus, the constructs should be considered experimental feasibility models, not clinical predictive patient avatars.

Study limitations include the three-patient cohort, availability of detailed longitudinal findings primarily from patient 1, the predominantly qualitative nature of the morphology, and the lack of paired molecular, histological, and microenvironmental validation. Future studies should include larger prospective cohorts, quantitative image analysis, viability data at the full replicate level, mechanical characterization of the bioink and direct comparison of parental tumors with printed constructs. Only after biological fidelity and technical reproducibility has been established

[Downloaded from mail.ijrr.com on 2026-11-11]

[DOI: 10.61186/ijrr.24.4.6]

should drug-response testing be implemented.

CONCLUSION

Patient-derived LGG cells were successfully integrated into GelMA-based 3D-bioprinted constructs that retained structural integrity and metabolic viability for up to 35 days. These results illustrate the technical feasibility of this platform to model adult IDH1-mutant low-grade gliomas. Further studies are needed to confirm molecular fidelity and reproducibility between patients and to apply this to drug response testing.

Acknowledgments**:** We thank ChangDu BioEng. & Therapy Co., Ltd. for their invaluable support in the development of 3D bioprinted primary LGG models and conducting cell viability assays.

Conflicts of interest**:** The authors declare no conflicts of interest.

Funding**:** Young Science and Technology Talent Support Program of Guangdong Precision Medicine Application Association(SKXRC2026148),Youth S&T Talent Support Programme of Guangdong Provincial Association for Science and Technology (GDSTA) (SKXRC2026148).

Ethical consideration**:** The study protocol was reviewed and approved by the Ethics Committee of the First Affiliated Hospital of Sun Yat-sen University. Written informed consent was obtained from all participants before the collection and experimental use of surgical tumor tissue. Additional consent was obtained for the use and publication of anonymized clinical, radiological, histopathological, and molecular data. All procedures were performed in accordance with the Declaration of Helsinki and relevant institutional and national ethical guidelines. (RN:QZYY-2026-049).

Author contribution**: B.H.,** Conceptualization, methodology, investigation, data curation, formal analysis, and drafting of the original manuscript. J.Y., Methodology, investigation, data collection, formal analysis, and drafting of the original manuscript. Z.Z., 3D-bioprinting methodology, technical support, experimental validation, and data interpretation. Y.L., Clinical data collection, radiological and pathological data organization, and manuscript revision. D.J., Conceptualization, supervision of the bioprinting experiments, resource provision, project administration, and critical revision of the manuscript. S.Y., Conceptualization, clinical supervision, project administration, funding acquisition, and critical revision of the manuscript. All authors reviewed and approved the final version of the manuscript and agreed to be accountable for the accuracy and integrity of the work.

Declaration of generative artificial intelligence use**:** No Artificial intelligence was used in writing and preparation of this manuscript.

REFERENCES

1. Jacob F, Salinas RD, Zhang DY, *et al.* (2020) A patient-derived glioblastoma organoid model and biobank recapitulates inter- and intra-tumoral heterogeneity. *Cell,* ***180****(1): 188-204.e22*.
2. Tang LW, Mallela AN, Deng H, *et al.* (2023) Preclinical modeling of lower-grade gliomas. *Front Oncol,* ***13****: 1139383*.
3. Zheng C, Wang P, Zhang D, *et al.* (2025) A novel organoid model retaining the glioma microenvironment for personalized drug screening and therapeutic evaluation. *Bioact Mater,* ***53****: 205-217*.
4. Abdullah KG, Bird CE, Buehler JD, *et al.* (2022) Establishment of patient-derived organoid models of lower-grade glioma. *Neuro Oncol,* ***24****(4): 612-623*.
5. Yuan M, White D, Resar L, *et al.* (2021) Conditional reprogramming culture conditions facilitate growth of lower-grade glioma models. *Neuro Oncol,* ***23****(5): 770-782*.
6. Neal JT, Li X, Zhu J, *et al.* (2018) Organoid modeling of the tumor immune microenvironment. *Cell,* ***175****(7): 1972-1988.e16*.
7. Murphy SV and Atala A (2014) 3D bioprinting of tissues and organs. *Nat Biotechnol,* ***32****(8): 773-785*.
8. Zhou M, Yue K, Zhao J, *et al.* (2025) Optimizing GBM organoid construction with hydrogel-based models: GelMA-HAMA scaffold supports GBM organoids with clonal growth for drug screening. *Cell Transplant,* ***34****: 09636897251347537*.
9. Yi HG, Jeong YH, Kim Y, *et al.* (2019) A bioprinted human-glioblastoma-on-a-chip for the identification of patient-specific responses to chemoradiotherapy. *Nat Biomed Eng,* ***3****(7): 509-519*.
10. Tang M, Jiang S, Huang X, *et al.* (2024) Integration of 3D bioprinting and multi-algorithm machine learning identified glioma susceptibilities and microenvironment characteristics. *Cell Discov,* ***10****(1): 39*.
11. Xie F, Sun L, Pang Y, *et al.* (2021) Three-dimensional bio-printing of primary human hepatocellular carcinoma for personalized medicine. *Biomaterials,* ***265****: 120416*.
12. Sun H, Sun L, Ke X, *et al.* (2024) Prediction of clinical precision chemotherapy by patient-derived 3D bioprinting models of colorectal cancer and its liver metastases. Adv Sci (Weinh), ***11****(2): e2304460*.
13. Du L, Zheng Z, Zhang K, *et al.* (2025) Exploring personalized prediction of clinical chemotherapy efficacy and revealing tumor heterogeneity using patient-derived 3D bioprinting gastric cancer models. *Mol Cancer,* ***24****(1): 259*.
14. Sun H, Wang Y, Sun M, *et al.* (2025) Developing patient-derived 3D -bioprinting models of pancreatic cancer. *J Adv Res,* ***74****: 165-174*.
15. Du L, Zheng Z, Wang Y, *et al.* (2026) Three-dimensional bioprinting of patient-derived gastrointestinal stromal tumor: a novel platform for precision oncology and drug response profiling. *J Nanobiotechnology,* ***24****(1): 64*.
16. WHO Classification of Tumours Editorial Board (2021) Central nervous system tumours. 5th ed. International Agency for Research on Cancer, Lyon, France.
17. Hubert CG, Rivera M, Spangler LC, *et al.* (2016) A three-dimensional organoid culture system derived from human glioblastomas recapitulates the hypoxic gradients and cancer stem cell heterogeneity of tumors found *in-vivo*. *Cancer Res,* ***76*** *(8): 2465-2477*.
18. Peng T, Ma X, Hua W, *et al.* (2025) Individualized patient tumor organoids faithfully preserve human brain tumor ecosystems and predict patient response to therapy. *Cell Stem Cell,* ***32****(4): 652-669.e11*.

[Downloaded from mail.ijrr.com on 2026-11-11]

[DOI: 10.61186/ijrr.24.4.6]

[DOI: 10.61186/ijrr.24.4.6] [Downloaded from mail.ijrr.com on 2026-11-11]